Final Progress Report

(27-02-2012 To 26-02-2014)

Project Title:-

Development of novel metal hydride-carbon nanomaterial based nanocomposites as anode electrode materials for Lithium ion battery

Objectives:-

The aim of this study is to develop metal hydride–carbon nanomaterial based nanocomposites as anode electrode materials for high capacity lithium ion battery and henceforth to develop high energy density, and good cyclic stability lithium ion battery.

Specific objectives:-

The details of the technical approach intended to be adopted in the execution of the project will be as follows:-

Milestone I

- *Synthesis of* nanosized metal hydrides (NMH)-carbon nanotubes (CNT) *hybridizing with G (NMH-CNT-G) nanocomposites*
- *Characterization of NMH-CNT hybridizing with G nanocomposites with XRD, Raman, SEM, AFM,TEM and HRTEM*
- *Processing of NMH-CNT-G nanocomposites based anode electrodes*
  {technical development of NMH-CNT-G nanocomposite and the NMH-CNT-G anode}

Milestone II

- *Studies of enhanced electrochemical performance and the enhanced cyclability of NMH-CNT-G as anode materials*
- *Development and testing of lithium ion battery with standard cathode electrode, nano metal hydride-carbon nanotubes-graphene based nanocomposites as anode materials and suitable organic electrolyte.*
  {technical development of battery with NMH-CNT-G anode for high energy density, and good cyclic stability}

Report Documentation Page

Form Approved
OMB No. 0704-0188

Public reporting burden for the collection of information is estimated to average 1 hour per response, including the time for reviewing instructions, searching existing data sources, gathering and maintaining the data needed, and completing and reviewing the collection of information. Send comments regarding this burden estimate or any other aspect of this collection of information, including suggestions for reducing this burden, to Washington Headquarters Services, Directorate for Information Operations and Reports, 1215 Jefferson Davis Highway, Suite 1204, Arlington VA 22202-4302. Respondents should be aware that notwithstanding any other provision of law, no person shall be subject to a penalty for failing to comply with a collection of information if it does not display a currently valid OMB control number.

1. REPORT DATE	2. REPORT TYPE	3. DATES COVERED
30 JUN 2014	**Final**	**27-02-2012 to 26-02-2014**

4. TITLE AND SUBTITLE
Development of novel metal hydride-carbon nanomaterial based nanocomposites as anode electrode materials for lithium ion battery

5a. CONTRACT NUMBER
FA23861214019

5b. GRANT NUMBER

5c. PROGRAM ELEMENT NUMBER

6. AUTHOR(S)
Sundara Ramaprabhu

5d. PROJECT NUMBER

5e. TASK NUMBER

5f. WORK UNIT NUMBER

7. PERFORMING ORGANIZATION NAME(S) AND ADDRESS(ES)
Alternative Energy Technology Laboratory,Indian Institute Of Technology Madras,Chennai 600 036,India,NA,NA

8. PERFORMING ORGANIZATION REPORT NUMBER
N/A

9. SPONSORING/MONITORING AGENCY NAME(S) AND ADDRESS(ES)
AOARD, UNIT 45002, APO, AP, 96338-5002

10. SPONSOR/MONITOR'S ACRONYM(S)
AOARD

11. SPONSOR/MONITOR'S REPORT NUMBER(S)
AOARD-124019

12. DISTRIBUTION/AVAILABILITY STATEMENT
Approved for public release; distribution unlimited

13. SUPPLEMENTARY NOTES

14. ABSTRACT
The aim of this study is to develop metal hydride?carbon nanomaterial based nanocomposites as anode electrode materials for high capacity lithium ion battery and henceforth to develop high energy density, and good cyclic stability lithium ion battery.

15. SUBJECT TERMS
enegy materials , Nanocomposites, lithium ion battery

16. SECURITY CLASSIFICATION OF:			17. LIMITATION OF ABSTRACT	18. NUMBER OF PAGES	19a. NAME OF RESPONSIBLE PERSON
a. REPORT	b. ABSTRACT	c. THIS PAGE			
unclassified	**unclassified**	**unclassified**	**Same as Report (SAR)**	**17**	

Work schedule *(Activity chart):-*

No	***Activity Description***	**1-12 months**	**13-22 months**	**23-24 months**
1	**Mile stone I:-** Recruitment of personal Processing MH, MWNT and graphene and characterization by SEM, TEM, HRTEM, Raman spectra. Synthesis of Nano MH-CNT hybridizing with G nanocomposites and characterization with XRD, Raman, SEM, AFM,TEM and HRTEM Studies of enhanced electrochemical performance and the enhanced cyclability of NMH-CNT-G as anode materials Technical development of NMH-CNT-G nanocomposite and the NMH-CNT-G anode			
2	**Mile stone II:-** Development and testing of lithium ion battery with standard cathode electrode, nano metal hydride–carbon nanotubes-graphene based nanocomposites as anode materials and suitable electrolyte. To optimize the materials for high energy density, and good cyclic stability of the battery			
3	Submission of final report, preparation of manuscripts and discussion on technology transfer.			

Final Report

Recently, graphene has emerged as an ideal material for different energy applications because of its high surface area and excellent electronic and thermal conductivity. The specific surface area of a single graphene sheet is 2630 m^2g^{-1}, which is quite higher than that of activated carbons and carbon nanotubes. To obtain a high yield of graphene sheets for various applications, graphene sheets are synthesized by chemical reduction of graphite oxide. These as-synthesized graphene sheets usually show low conductivity due to the presence of oxygen functional groups and large agglomeration by van der Waals attraction. Li ions experience difficulty in intercalating between restacked graphene sheets and end up accumulating at the top and bottom surfaces of the agglomerates. This limits the Li storage capacity of graphene sheets despite a high theoretical surface area and thus lower specific capacity values are observed. In this regard, the incorporation of multiwalled carbon nanotubes (MWNTs) along with the graphene sheets prevents the restacking of graphene sheets, while also enhances the conductivity of the nanocomposite. The electrical conductivity of MWNTs (~10000 S m^{-1}) is two orders higher than that of reduced graphene sheets (100–200 S m^{-1}). Chemical modification of graphene and MWNT surfaces is necessary for strengthening the interaction between them artificially, which in turn may enhance the electron and Li ion transport in this hybrid nanostructure. This aspect is investigated in the present work wherein we report a simple approach to synthesize graphene-MWNT nanocomposite.

The MWNTs were synthesized by chemical vapor deposition technique (CVD) over rare earth metals based $MmNi_3$ (Mm = Mischmetal; a mixture of rare earth elements) alloy hydride catalyst using acetylene gas as the carbon precursor as reported earlier[1]. The as-synthesized MWNTs were subjected to air oxidation to remove carbonaceous impurities followed by acid treatment to remove the $MmNi_3$ catalyst particles. For further functionalization, the purified MWNTs were refluxed with concentrated H_2SO_4 and HNO_3 in the ratio (3:1) for 24 h at 80°C, followed by washing, filtering and drying at 70°C. The sample was labeled as *f*-MWNTs.

Graphite oxide (GO) was prepared from natural graphite using Hummers' method from graphite powder[2]. In a typical synthesis, graphite powder (2 g) was added to concentrated H_2SO_4 (46 mL) while being continuously stirred in an ice bath. Next, $NaNO_3$ (1 g) and $KMnO_4$ (6 g) were added gradually and successively. The suspension was removed from the ice bath and was allowed to come to room

temperature. Next, water (92 mL) was added to the above mixture. After 15 min, warm water (280 mL) was added to dilute the mixture. Following this, H_2O_2 (3%) was added until the solution turned bright yellow. The suspension was filtered and repeatedly washed with warm water. The residue was diluted using water and the resulting suspension was centrifuged. The final product was dried under vacuum at 60°C and stored in vacuum desiccators until further use. Graphene was prepared by the solar exfoliation of graphite oxide as reported by us earlier[3]. For this, GO powder (about 300 mg) was spread in a glass petridish and a convex lens was used to focus the solar radiation on it. The rapid exfoliation of GO occurs within few seconds under the focused solar radiation. As the focused spot of sunlight interacts with the GO powder, rapid volume expansion accompanied by a change in color (from brownish to black) was observed indicating the swift reduction of GO to graphene. The sample was labeled as SEG for solar-exfoliated graphene. The power of the focused radiation ranged from 1.77-2.03 W and temperature range was 250-300°C.

The as-synthesized SEG was functionalized with the polyelectrolyte PDDA by the following method. SEG (about 200 mg) was initially dispersed in DI water (800 mL) by ultrasonication in the presence of PDDA (0.5 wt %), which served as the functionalizing polyelectrolyte and yielded a stable dispersion of graphene sheets. During the functionalization process, NaCl was added. The presence of NaCl drastically affects the polymeric chains' configuration in polyelectrolyte solutions and promotes the functionalization. The solution was then filtered and washed several times to remove the unreacted PDDA in the solution followed by drying in vacuum oven at 70 °C for 24 h. The PDDA functionalized graphene was labeled as '*p*G'. To prepare the hybrid nanostructure of MWNT and graphene, *f*-MWNT and *p*G were simply ultrasonicated in DI water in the ratio (1:1) for one 1 h followed by stirring for 12 h. The sample was then filtered and dried at 50 °C in vacuum oven. The final sample was labeled as '*p*G-*f*-MWNT'.

Fig. 1 illustrates the scheme followed for the synthesis of *p*G-*f*-MWNT hybrid nanostructure. In the present case, when positively charged surface of graphene and negatively charged surface of *f*-MWNTs are mixed together by ultrasonication in DI water, both get well dispersed in water because of surface functionalization and electrostatic interaction among themselves. The surface charges, therefore, promote the formation of layered structures. The MWNTs thus also play the role of spacers forming a sandwiched layer between the graphene sheets. As like charges repel each other, the self-agglomeration of the graphene sheets (charged positively) and *f*-MWNTs (charged negatively) in solution is also prevented.

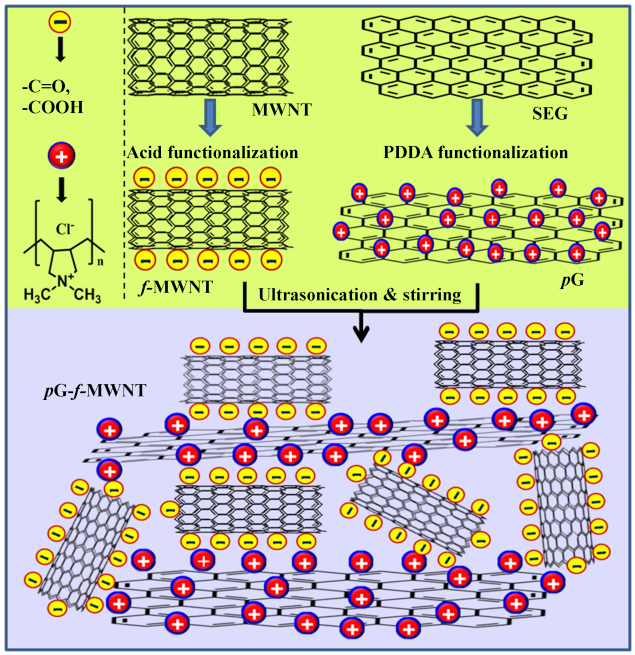

Fig. 1. Scheme outlines the synthesis procedure adopted for synthesizing graphene-MWNT nanocomposite

Fig. 2 presents the powder X-ray diffractograms of (a) graphite (Gr), (b) GO, (c) SEG, (d) MWNTs and (e) *p*G-*f*-MWNT, respectively. For graphite an intense crystalline peak occurs at a 2θ value of 26.73°, which is the characteristic peak of the (002) plane in hexagonal graphite with a *d*-spacing of 0.334 nm. Upon oxidation of graphite, the (002) peak shifts to 10.54° as seen in Fig. 2(b). An increase in the interlayer spacing to 0.84 nm is observed, which may be attributed to the intercalation of oxygen containing functional groups in between the graphite sheets. After exfoliation of GO with focused solar radiation at ~ 300 °C, the 10.54° peak disappears and a broad peak ranging from 15° to 30° is observed (Fig. 2(c)). This peak, as in the case of graphite, arises due to the carbon (002) plane of the hexagonal structure. The broadening, however, indicates the presence of disorder along the *c*-axis. The interlayer spacing decreases to 0.374 nm, which suggests the removal of oxygen functional groups and water from the layers during solar exfoliation. Both graphene and MWNTs exhibit the hexagonal structure of graphite, and hence, the presence of (002) plane is observed in their hybrid nanocomposite. The sharp peak is attributed to the presence of MWNTs, while the broadened feature from 17°-25° is due to the loose stacking of hexagonal sheets in graphene. An increase in the *d*-spacing of *p*G-*f*-MWNT hybrid structure is observed. This suggests that the packing of graphene sheets along the (002) direction is loosened due the presence of MWNTs that play the role of 'spacers'. The increase in the *d*-spacing of *p*G-*f*-MWNT hybrid structure (0.341

nm) as compared to MWNT suggests that MWNTs strongly interact with graphene sheets and thus act as spacers in between them preventing their agglomeration. The *p*G-*f*-MWNT hybrid composite is further characterized by Raman spectra, FTIR, SEM, TEM and HRTEM images and nitrogen adsorption-desorption measurements as shown in figures 3-6. Table I shows the BET surface area, average pore size and pore volume calculated for MWNT, SEG and pG-f-MWNT.

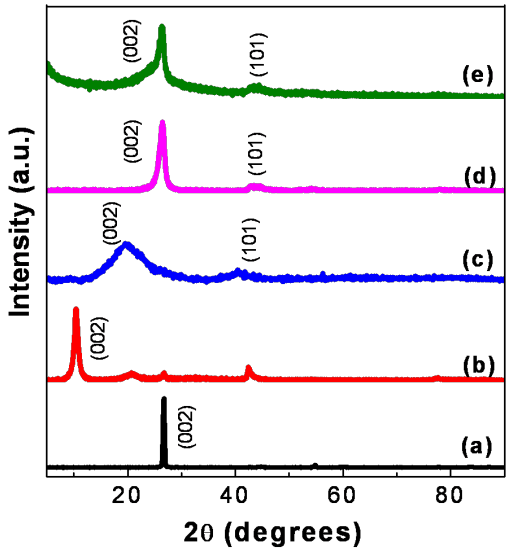

Fig. 2. X-ray diffractograms of (a) graphite, (b) graphite oxide, (c) solar exfoliated graphene, (d) multiwalled nanotubes, and (e) graphene-multiwalled carbon nanotubes composite acquired in the 5-90° range

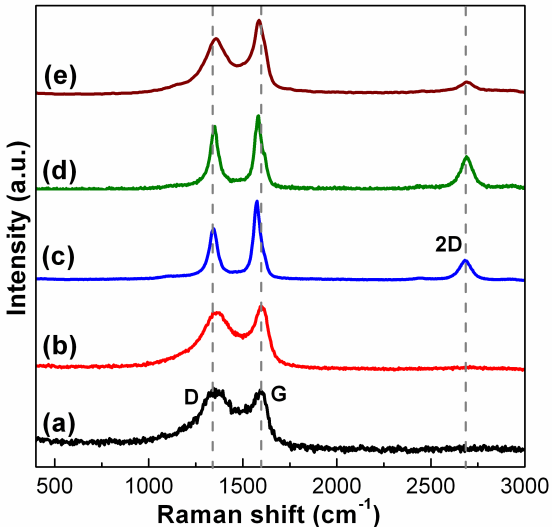

Fig. 3. Raman spectra showing the positions of G-, D- and 2D-bands in case of (a) solar exfoliated graphene, (b) PDDA functionalized graphene, (c) multiwalled carbon nanotubes, (d) acid functionalized multiwalled carbon nanotubes, and (e) graphene-multiwalled carbon nanotubes composite

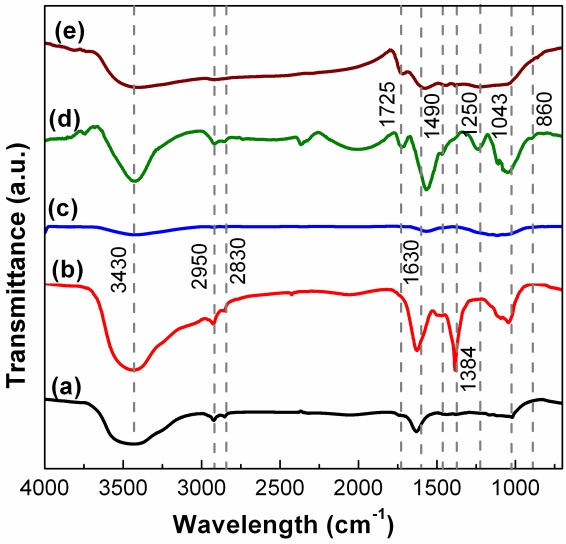

Fig. 4. FTIR spectra corresponding to (a) multiwalled carbon nanotubes, (b) acid functionalized multiwalled carbon nanotubes, (c) solar exfoliated graphene, (d) PDDA functionalized graphene, and (e) graphene-multiwalled carbon nanotube composite

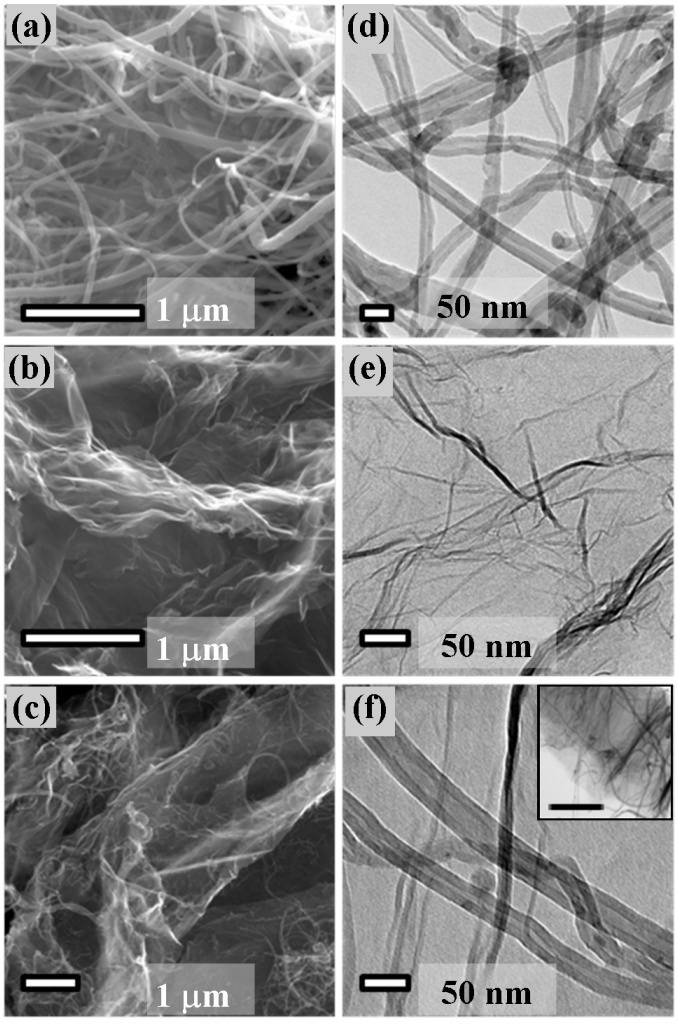

Fig. 5. Scanning and transmission electron micrographs of multiwalled carbon nanotubes (a,d), solar exfoliated graphene (b,e), and graphene-multiwalled carbon nanotube composite (c,f), respectively display the morphology of the corresponding samples. Inset in (f) shows a large area of the graphene-multiwalled carbon nanotube composite where wrapping of nanotubes between graphene sheets is visible. Scale bar corresponds to 1 μm

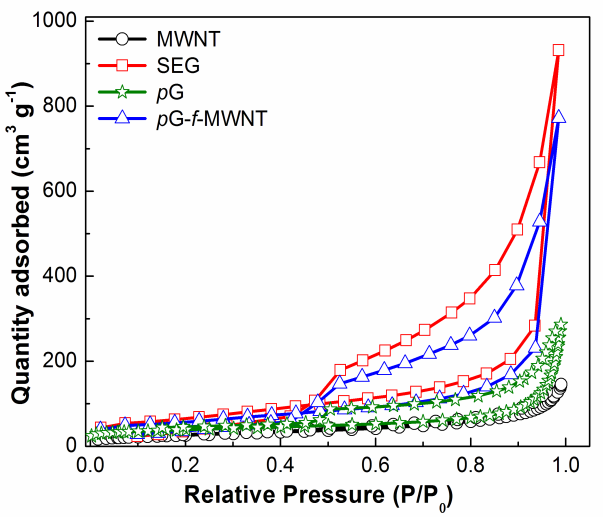

Fig. 6. Nitrogen adsorption-desorption isotherms of acid functionalized multiwalled carbon nanotubes, solar exfoliated graphene, PDDA functionalized graphene, and graphene-multiwalled carbon nanotube composite

Table I. *The values of BET surface area, average pore size and pore volume calculated for MWNT, SEG and pG-f-MWNT.*

Sample	S_{BET} (m^2 g^{-1})	Average pore size (nm)	Pore volume (cm^3 g^{-1})
MWNT	92	4.20	0.22
SEG	236	43.80	1.35
*p*G	135	10.42	0.44
*p*G-*f*-MWNT	203	42.86	1.13

Polyelectrolyte PDDA was used to modify the HEG surface with positively charged ions by the previous reported method[4]. Briefly, 200 mg HEG was initially dispersed in DI water by ultrasonication. PDDA (0.5 wt %) and NaCl was added to the earlier solution subsequently. The amount of NaCl controls the construction of the polymeric chains in the solution. The solution was then washed to remove the unused PDDA several times and dried at 70 ˚C to get functionalised graphene (pG). The fusion of *f*-MWNTs and pG was achieved in a ratio of 1:1 by ultrasonication in DI water followed by stirring for uniform dispersion. The suspension was filtered and dried in vacuum oven at 50 ºC. Dried sample was written off as pG–f-MWNT.

SnO_2 nanoparticles were dispersed over pG–*f*-MWNT by a modified polyol reduction method. Briefly, 100 mg pG–*f*-MWNT was dispersed in a solution of ethylene glycol and water (1:1). Required amount of $SnCl_2 .2H_2O$ was added to this dispersion and stirred for 12 h. 1 M NaOH and 0.1 M $NaBH_4$ solution was added to this suspension drop wise as reducing agent and the solution was stirred for another 12 h. The suspension was filtered, washed with D I water, dried and annealed at 200 ˚C for 1 h in ambient atmosphere to get SnO_2(pG-*f*-MWNT).

The X-ray diffraction (XRD) measurements were performed with a PANalytical X'Pert Pro X-ray diffractometer with nickel filtered Cu-K_α radiation as the X-ray source. The pattern was recorded in the 2θ range of 5 º – 90 º with a step size of 0.016 º. The vibrational characteristics of the samples were analyzed via Raman spectroscopy using 532 nm laser (Witec Alpha 300) as the excitation source in the range 500–3000 cm^{-1}. Functional group identification was done using a PERKIN ELMER FT-IR spectrometer in the range of 500–4000 cm^{-1} using KBr pellet method. The morphology of the samples was characterized by field emission scanning electron microscope (FESEM, FEI QUANTA3D), and transmission electron microscope (FEI Technai G^2 20 STWIN, 200 keV).

Fig. 7 presents the powder X-ray diffractograms of the materials invested in this report. An intense crystalline peak of Fig. 7a at 26.68 ° represents the high crystallinity of used graphite material with a d spacing of 0.334 nm. This (002) peak shifts to 10.84 ˚ as the d spacing increased to 0.84 nm due to incorporation of various functional groups upon oxidation as seen in Fig. 7(b). In the hydrogen reduction technique this shifted peak disappears and a broad peak from 15 º to 38 º appears. The broadening in this (002) plane of the hexagonal structure explains the presence of disorder along the c-axis due to the random orientation after exfoliation with a decrement in interlayer spacing. This reduction in spacing

suggests the elimination of oxygen containing functional groups in HEG (Fig. 7c). The MWNTs of Fig. 7d show the relatively sharp hexagonal graphitic peak at (002) assuring the long range order present in the system. Fig. 7e shows the XRD pattern of hybrid nanostructure pG–f-MWNT with a broadened feature and a sharp peak. The broadened characteristic represents the disturbed loose stacking graphene sheets and sharp peak is recognized as the signature of MWNTs. An increase in the d-spacing of pG–*f*-MWNT hybrid structure is observed. The suggestion of MWNTs acting as spacers is verified by the increased d spacing of the composite structure to 0.34 nm. The XRD pattern of SnO_2(pG-*f*-MWNT) nanocomposite can be seen from Fig 7f, which confirms the presence of SnO_2 together with carbon. It showed SnO_2 crystallized in a tetragonal structure (JCPDS no: 41-1445) and at 26 °, the broadened (002) peak of pG-*f*-MWNT is merged with the (110) peak of SnO_2.

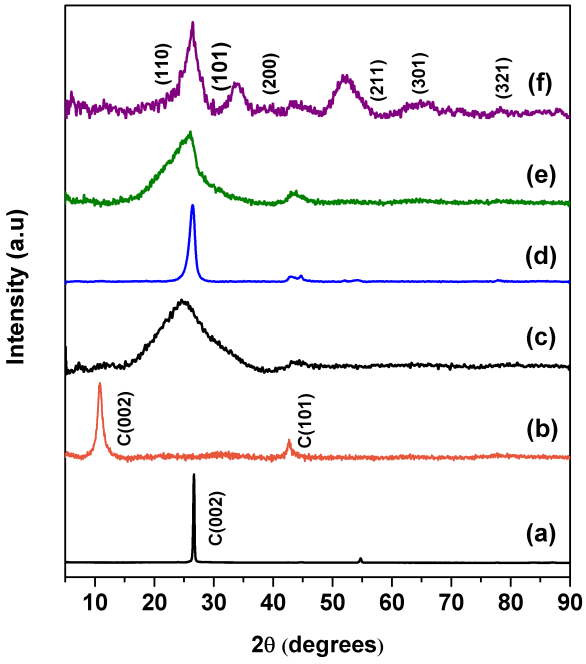

Fig. 7. X-ray diffractograms of (a) graphite, (b) GO, (c) HEG, (d) *f*-MWNTs, (e) pG–*f*-MWNT and (f) SnO_2 (pG–*f*-MWNT)

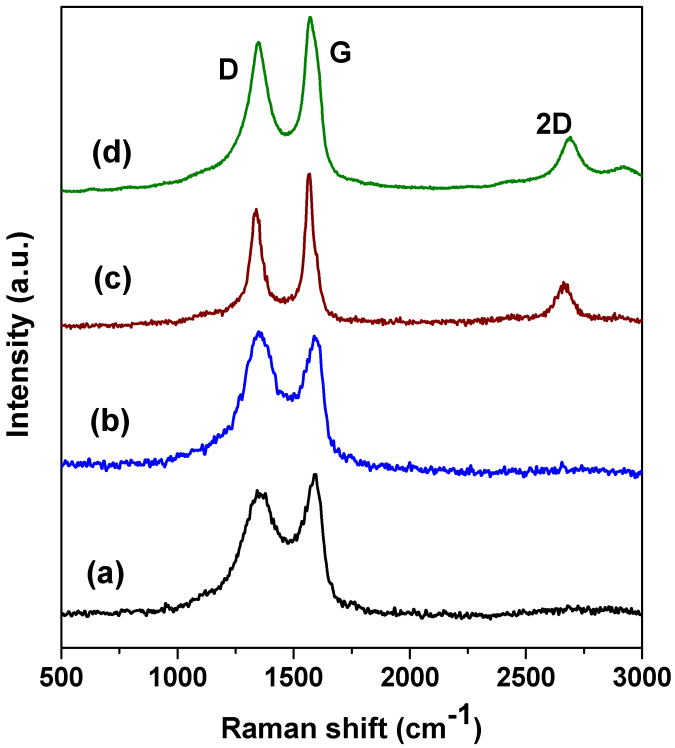

Fig. 8. Raman spectra of (a) HEG (b) pG (c) *f*-MWNTs, and (d) pG- *f*-MWNTs

Raman spectra of (a) HEG (b) pG (c) *f*-MWNT and (d) pG–*f*-MWNTs are shown in Fig. 8. For graphitic materials, G band arises due to the Raman active E_{2g} mode and D band from the defects of the material. The ratio of the intensities of D and G bands (I_D/I_G) is utilised to predict the existence of defects within the samples, which is shown for all the samples in the Table 2. Broad G band at 1588 cm^{-1} and D band at 1355 cm^{-1} was observed for HEG in fig 8a. The increment in the I_D/I_G ratio for pG compared to HEG is attributed to the functionalization with the polyelectrolyte PDDA on graphene, but the small change indicates that the process does not induce many defects on the graphene surfaces. A forward shift in G band can be observed from HEG (1588) to pG (1592), signifying the occurrence of electron transfer from graphene sheets to the adsorbed PDDA[5]. *f*-MWNTs exhibit the G and D band at 1566 cm^{-1} and 1340 cm^{-1} respectively as seen from Fig 8c. The pG- *f*-MWNTs shows a G band at 1572 cm^{-1} and D-band at 1348 cm^{-1}. As can be seen from Table 3, the I_D/I_G ratio for pG- *f*-MWNTs is increased compared to *f*-MWNT, attributing to the presence of disordered pG sheets.

Material	HEG	pG	*f*-MWNT	pG-*f*-MWNT
I_D/I_G *ratio*	0.89	1.02	0.76	0.87

Table 2: The I_D/I_G ratio of the different samples estimated from their corresponding Raman spectrum

Fig. 9 shows the FTIR spectrum for (a) HEG (b) pG (c) P-MWNT, (d) *f*-MWNT and (e) pG–f-MWNT (f) SnO_2(pG-*f*-MWNT) for the functional groups present in the system. 2922 cm^{-1} peak of Fig 9a corresponds to the $–CH_2$ stretching vibrations suggesting a redecoration in the carbon basal planes for HEG. Broadened peak for all the samples around 3440 cm^{-1} represents the –OH stretching vibrations. No other oxygen containing functional groups can be detected in Fig 9a, suggesting removal of them in the form of water vapour or carbon dioxide due to hydrogen reduction. PDDA modified HEG showed a small peak around ~860 cm^{-1} and 1500 cm^{-1} in Fig. 9b suggests the presence of C–N bond in the HEG adsorbed PDDA[5].

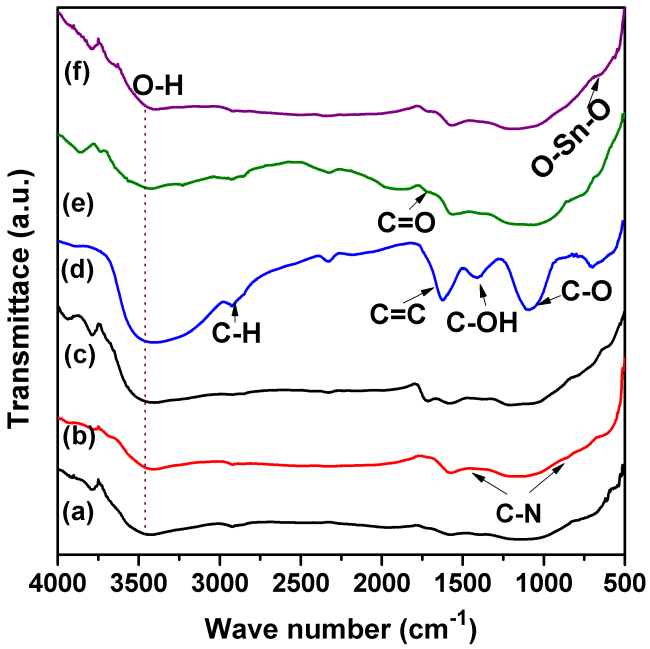

Fig. 9. FTIR spectrum obtained for (a) HEG (b) pG (c) p-MWNT, (d) *f*-MWNT (e) pG–*f*-MWNT and (f) SnO_2(pG-*f*-MWNT)

FT-IR spectra of Fig. 9d for *f*-MWNT shows enhancement in the attached functional groups as compared to P-MWNT (Fig. 9c). The band around 2950 cm^{-1} is attributed to stretching of C–H bond and the peak at 1630cm^{1} is due to the C=C stretching mode of multiwalled carbon nanotubes. The peaks at 1388 cm^{-1} and 1070 cm^{-1} are due to C–OH and C–O stretching vibrations respectively. C=O vibration is represented in 1725 cm^{-1} peak. O-Sn-O anti-symmetric stretching was found around 660 cm^{-1} for Fig. 9f. This mode confirms the incorporation of SnO_2 nanoparticles on the support material[6, 7].

Fig. 10 shows the SEM images of the support material pG-*f*-MWNT and SnO_2 decorated over the composite material. The images clearly demonstrate the proposed structure of MWNTs interwoven with graphene sheets.

TEM image of pG-*f*-MWNT in Fig. 11a shows the inner hollowness of MWNTs and uniform dispersion of these MWNTs with polymer functionalised graphene sheets. Fig. 11b depicts the uniform dispersion of SnO_2 nanoparticles on graphene- carbon nanotubes hybrid structure. The particle size of the SnO_2 nanoparticle is approximately less than 5 nm.

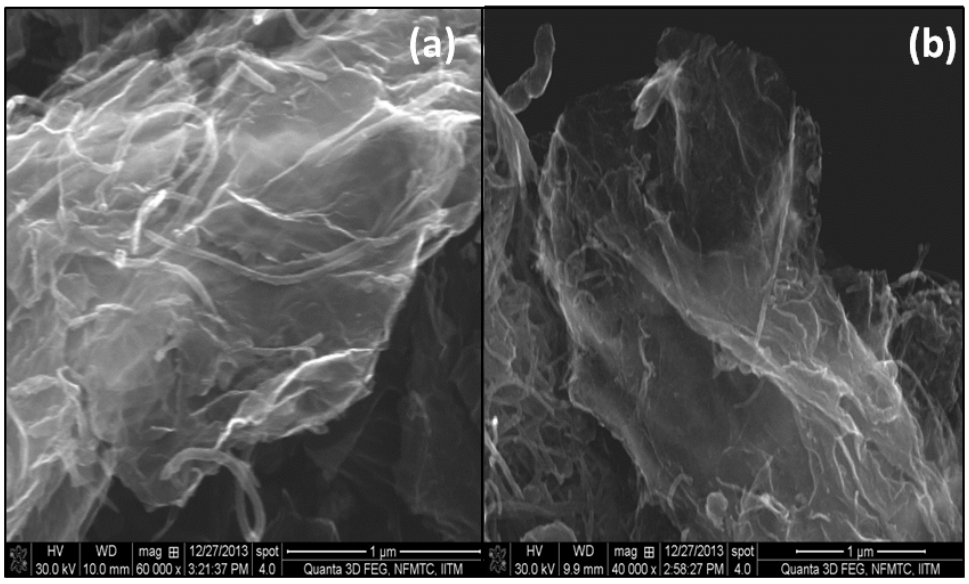

Fig. 10. (a) Scanning electron micrographs of (a) pG-*f*-MWNT and (b) SnO_2-(pG-*f*-MWNT)

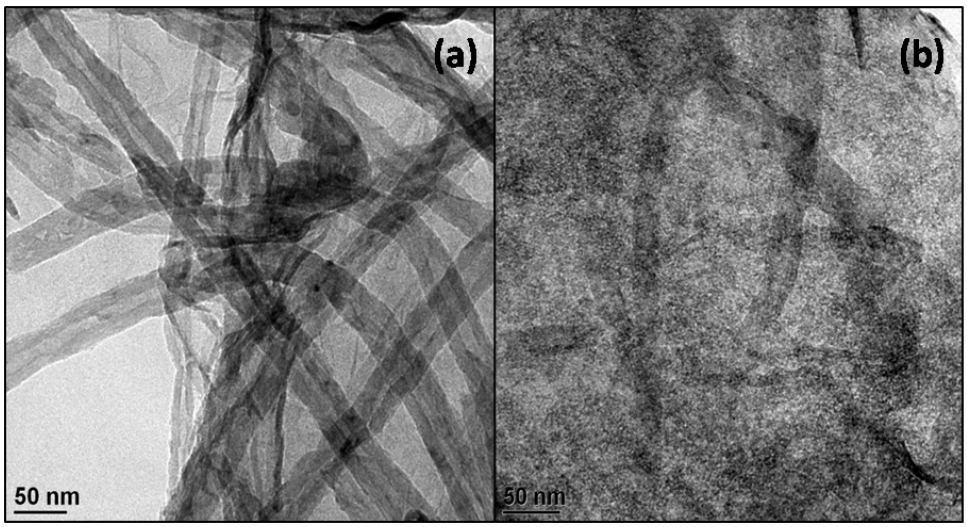

Fig. 11. Transmission electron micrographs of (a) pG-*f*-MWNT and (b) SnO_2(pG-*f*-M WNT)

To enhance capacity of the carbon hybrid structure as reported[4] earlier SnO_2 nanoparticles were dispersed on the support (pG–f-MWNT). As discussed earlier the negatively charged oxygen functional groups on MWNTs electrostatically interact with positively charged ions or molecules on graphene surface. These surface charges allowed a strong bond within the formed layered structure in which MWNTs act as conducting spacer between graphene sheets preventing the self agglomeration. The increased surface area of the composite compared to MWNT offers more active sites to SnO_2, which get uniformly distributed over the homogeneous layered structure.

The working electrodes were prepared by mixing active material (90 wt %) i.e. SEG or *p*G-*f*-MWNT or SnO_2 (pG–*f*-MWNT) hybrid structure with polyvinylidene fluoride (PVDF, 10 wt %) binder dissolved in *N*-methyl-2-pyrrolidinone. No conductive carbon was added for making the slurry. After coating the above slurries on Cu foils, the electrodes were dried at 120 °C in vacuum for 6 h to remove the solvent before pressing. The electrodes were then pressed and cut into disks (12 mm in diameter). Electrochemical measurements were carried out using Swagelok type two-electrode cell with lithium metal as the counter/reference electrode, Celgard 2400 membrane separator, and $LiPF_6$ (1 M) electrolyte solution dissolved in a mixture of ethylene carbonate (EC) and dimethyl carbonate (DMC) (EC/DMC, 1:1 v/v). The cells were assembled in an argon-filled glove box. Galvanostatic charge-discharge measurements were carried out using a Solatron electrochemical workstation between 3 and 0.05 V vs. Li^+/Li at room temperature.

Fig. 12 shows the galvanostatic charge-discharge profiles for (a) SEG (b) *p*G-*f*-MWNT at the current density of 90 mA g^{-1} in the voltage range 3-0.05V (vs. Li^+/Li). The initial charge and discharge capacities for SEG were 443 mAh g^{-1} and 588 mAh g^{-1}, respectively. At the same time for *p*G-*f*-MWNT hybrid structure, initial charge and discharge capacities were 912 mAh g^{-1} and 1371 mAh g^{-1}, respectively. The large initial capacity losses were observed for SEG and *p*G-*f*-MWNT after the first cycle. These may be attributed to the lithium ion consumption during the electrolyte decomposition and formation of solid electrolyte interface film around the electrodes with large surface areas.[25] After the 30th and the 100th cycle SEG yielded a reversible discharge capacity of 257 mAh g^{-1} and 220 mAh g^{-1}, respectively, which are comparable or higher than that of previously reported reversible capacity values of graphene and MWNT.[3, 25] Ali *et al.* have shown that graphene powder and graphene paper can give reversible capacities of 84 and 288 mAh g^{-1} respectively at 50 mA g^{-1}.[25] The reported reversible capacities of MWNT vary from 200-300 mAh g^{-1} in the current density range 10-50 mA g^{-1}.[3, 26] It is expected that the reversible capacity should be higher at a lower current density. Yoo et al. have investigated the Li storage by graphene nanosheet family in detail where the investigated specimens exhibit distinct charge-discharge profiles as compared to crystalline graphite owing to the presence of different Li storage sites. The charge-discharge profiles reveal three different regions in case of carbon nanomaterials namely; Li deposition in micropores, intercalation of Li and Li binding to the sites of hydrogen terminated dangling bonds.[6,27] In the present work, charge-discharge profiles of SEG and *p*G-*f*-MWNT do not reveal any plateau shapes suggesting that the initial Li deposition in pores does not take place in either case. Thus, capacity of the potential region lower than 0.5 V (vs. Li/Li^+) is attributed to the intercalation of lithium into the graphene and MWNT layers. The cyclic stability of the SEG and *p*G-*f*-MWNT anode materials was tested by running the cells at a current density of 90 mA g^{-1} for 100 cycles and Fig. 13 shows their comparison. After the 30th and the 100th cycles, the *p*G-*f*-MWNT hybrid nanostructure gives reversible discharge capacities of 813 mAh g^{-1} and 768 mAh g^{-1}, respectively, yielded a 59 % and 56 % retention of the initial capacity. At the same time, for graphene it was 43.7% and 37.4%, respectively. The reversible discharge capacity of (graphene-MWNT) after 30th and 100th cycles is 2.16 and 2.5 times higher than that of pure graphene and previously reported reversible discharge capacities of graphene-MWNT composite.

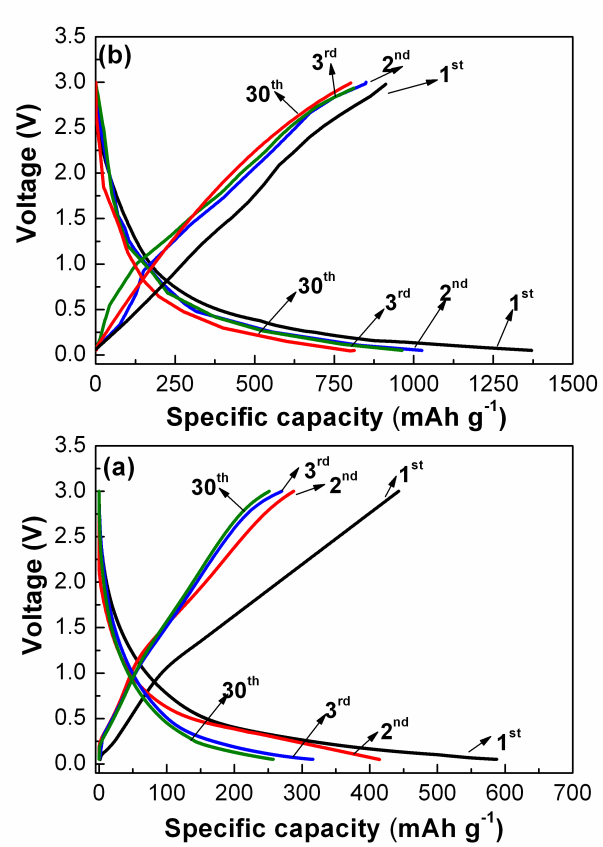

Fig. 12. Galvanostatic charge-discharge curves for (a) solar exfoliated graphene and (b) graphene-multiwalled carbon nanotube composite in the voltage range of 0.05-3 V vs. Li/Li^+ electrode acquired at a current density of 90 mA g^{-1}

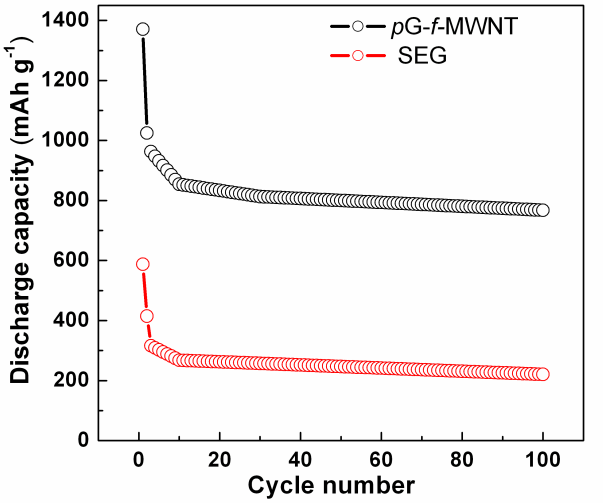

Fig. 13. Cyclic stability of solar exfoliated graphene and graphene-multiwalled carbon nanotube composite tested up to 100 cycles at a current density of 90 mA g^{-1}

Thus the novel hybrid nanomaterial comprising of PDDA modified solar exfoliated graphene and negatively surface charged MWNTs exhibits a good specific capacity and cyclic stability. The SEG and *p*G-*f*-MWNT hybrid nanostructure gave a Li-ion battery discharge capacity of 220 mAh g^{-1} and 768 mAh g^{-1} after 100 cycles. The high performance of the *p*G-*f*-MWNT hybrid nanostructure is attributed to the strong electrostatic interaction between positively charged surface of graphene sheets and negatively charged surface of MWNTs, which prevent the restacking of graphene layers offering a shortened diffusion distance for Li^+ ions and electrons.

Publication

1. *Synthesis of graphene-multiwalled carbon nanotubes hybrid nanostructure by strengthened electrostatic interaction and its lithium ion battery application, Journal of Material Chemistry, 2012,* ***22****, 9949*
2. *Development of novel SnO_2 dispersed graphene-multiwalled carbon nanotubes hybrid nanostructure as anode electrode materials for lithium ion battery (to be communicated)*

References

1. A. L. M. Reddy, M. M. Shaijumon and S. Ramaprabhu, *Nanotechnology*, 2006, 17, 5299.
2. W. S. Hummers and R. E. Offeman, *Journal of the American Chemical Society*, 1958, 80, 1339-1339.
3. A. Kaniyoor, T. T. Baby and S. Ramaprabhu, *Journal of Materials Chemistry*, 2010, 20, 8467-8469.
4. B. P. Vinayan, R. Nagar, V. Raman, N. Rajalakshmi, K. S. Dhathathreyan and S. Ramaprabhu, *Journal of Materials Chemistry*, 2012, 22, 9949-9956.
5. S. Wang, D. Yu, L. Dai, D. W. Chang and J.-B. Baek, *ACS Nano*, 2011, 5, 6202-6209.
6. F. Gu, S. Fen Wang, C. Feng Song, M. Kai Lü, Y. Xin Qi, G. Jun Zhou, D. Xu and D. Rong Yuan, *Chemical Physics Letters*, 2003, 372, 451-454.
7. F. Tuinstra and J. L. Koenig, *The Journal of Chemical Physics*, 1970, 53, 1126-1130.
8. B. Zhang, Q. B. Zheng, Z. D. Huang, S. W. Oh and J. K. Kim, *Carbon*, 2011, 49, 4524-4534.
9. G. Wang, B. Wang, X. Wang, J. Park, S. Dou, H. Ahn and K. Kim, *Journal of Materials Chemistry*, 2009, 19, 8378-8384.
10. S.-M. Paek, E. Yoo and I. Honma, *Nano Letters*, 2008, 9, 72-75.
11. J. Yao, X. Shen, B. Wang, H. Liu and G. Wang, *Electrochemistry Communications*, 2009, 11, 1849-1852.